CHEMISTRY OF MATERIALS

Article

pubs.acs.org/cm

# Unraveling the Origin of Visible Light Capture by Core–Shell $TiO_2$ Nanotubes

Jun Li,[†] Chang-Hai Liu,[‡] Xia Li,[§] Zhi-Qiang Wang,[†] Yu-Cheng Shao,[∥,⊥] Sui-Dong Wang,[‡] Xue-Liang Sun,[§] Way-Faung Pong,[⊥] Jing-Hua Guo,[∥,#] and Tsun-Kong Sham*[,†,¶]

[†]Department of Chemistry and [¶]Soochow University-Western University Centre for Synchrotron Radiation Research, University of Western Ontario, 1151 Richmond Street, London, Ontario N6A 5B7, Canada

[‡]Institute of Functional Nano and Soft Materials (FUNSOM) and Soochow University-Western University Joint Centre for Synchrotron Radiation Research, Soochow University, Suzhou, Jiangsu 215123, Peoples' Republic of China

[§]Department of Mechanical and Material Engineering, University of Western Ontario, London, Ontario N6A 5B9, Canada

[∥]Advanced Light Source, Lawrence Berkeley National Laboratory, Berkeley, California 94720, United States

[⊥]Department of Physics, Tamkang University, New Taipei City 25137, Taiwan, The Republic of China

[#]Department of Chemistry and Biochemistry, University of California, Santa Cruz, California 95064, United States

Supporting Information

**ABSTRACT:** A black $TiO_2$ nanotube (NT) heterostructure with an anatase-core and an amorphous-shell has been synthesized by $NH_3$ annealing of amorphous NT grown by the anodization of a Ti substrate. Remarkable photoabsorption behavior of these black $TiO_2$ NTs is observed: strong absorption throughout the entire optical wavelength region from ultraviolet to near-infrared. X-ray absorption near-edge structure (XANES), X-ray photoelectron spectroscopy (XPS) and resonant inelastic X-ray scattering (RIXS) have been used to elucidate the origin of this spectacular light capture phenomenon. Surface-sensitive XANES recorded in total electron yield and XPS show that the surface layer is amorphous with a chemical composition approaching that of $Ti_4O_7$. Bulk-sensitive XANES using X-ray partial fluorescence yield and Ti 2p RIXS confirm the presence of a rich amount of $Ti^{3+}$ in the crystalline bulk (core of the NT with anatase structure) of black $TiO_2$ NTs, which exhibits a dispersive d-d energy loss at ~2 eV corresponding to the broad visible light absorption at ~600 nm. Our results suggest that the extraordinary photoabsorption behavior of these black $TiO_2$ NTs is due to the stabilization of $Ti^{3+}$ in this special N-doped core–shell assembly having structure varying between $TiO_2$ (bulk anatase) and $Ti_4O_7$ (surface, amorphous).

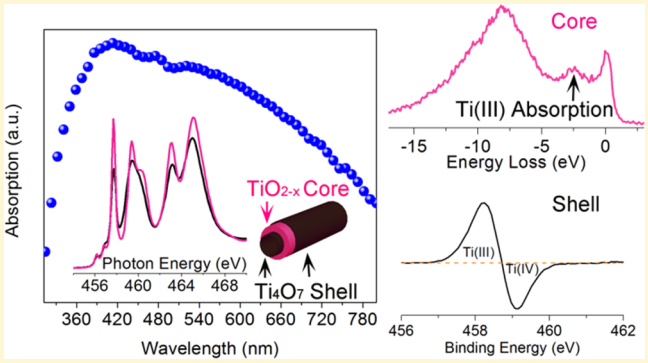


## INTRODUCTION

As one of the most promising photocatalysts, $TiO_2$ has recently been treated as one of the foremost significant materials in the environmental and energy realm.[1−4] However, the large band gap of $TiO_2$ (~3 eV) only allows absorption in the ultraviolet (UV) region and thus constitutes a severe limitation for its application in photocatalysis, as UV just holds a small fraction (~5%) of solar energy compared to visible (~43%) and near-infrared (~52%) regions.[2,5] In developing novel $TiO_2$ nanostructures to extend their photoabsorption to the visible and near-infrared regions, narrowing the band gap of $TiO_2$ by properly altering the band energy will establish a benchmark for engineering sunlight-driven functional materials.

Generally, chemical doping by appropriate introduction of metal and nonmetal impurities is a popular way for tailoring the $TiO_2$ band gap.[1,3,6,7] Among them, N doping is a typical example and N-doped $TiO_2$ indeed has shown some success in extending its optical response to the visible region.[3,8] The involvement of substitutional N doping is considered to be indispensable for $TiO_2$ band gap narrowing by upshifting the valence band maximum as a result of the mixing between N 2p and O 2p states.[3] Moreover, synergistic interactions between N dopant and concomitant $Ti^{3+}$ is also believed to be key for improved photoabsorption and associated photoactivity of N-doped $TiO_2$.[3,8,9] Nevertheless, insufficient visible and near-infrared absorption of N-doped $TiO_2$ reported so far makes it less than satisfactory for solar energy utilization.[1]

Recently, Chen et al.[1] applied high pressure hydrogen treatment to obtain the core–shell black $TiO_2$ of which the introduction of disorder on the surface shows its decisive role in reducing the $TiO_2$ band gap, resulting in considerable improvement in visible and infrared absorption of black $TiO_2$. Since then, vast efforts have been made to investigate this type

Received: April 25, 2016
Published: May 24, 2016





DOI: 10.1021/acs.chemmater.6b01673
Chem. Mater. 2016, 28, 4467−4475

of disordered $TiO_2$ nanostructure and to reveal the origin of visible light absorption.[1,10−14] The creation of two band tail states by surface disorder associated with their merging with the valence band maximum and conduction band minimum of $TiO_2$ has long been believed to be responsible for the band gap narrowing of highly reduced black $TiO_2$.[1,14] However, this nonspecific ascription does not pinpoint the chemical nature of the outermost amorphous layer, and the mechanism for the optical absorption remains inconclusive. Alternatively, a very recent report by Tian et al.[12] provides evidence of $Ti_2O_3$ formation in the surface layer via interstitial diffusion of Ti ions from the bulk rutile $TiO_2$. The distinct points are the narrow band gap of $Ti_2O_3$ and its robust structure for preserving surface $Ti^{3+}$.[8,10,12] However, two issues still need to be addressed. First, the amorphous layer grown on top of the anatase $TiO_2$ is the one that exhibits superior photoactivity, and the surface amorphization behavior between anatase and rutile is certainly different.[1,13] Therefore, it is crucial to understand the chemical nature of the surface disordered layer above the anatase $TiO_2$. Second and more importantly, the amorphous shell with a single phase on its own could not achieve broad light absorption at both the visible and near-infrared regions,[1] so the synergistic interaction between the amorphous shell and anatase core corresponding to the enhanced photoabsorption of black $TiO_2$ needs to be clarified.

In this work, we show that $NH_3$ annealing of vertically aligned $TiO_2$ nanotubes (NTs) in the amorphous phase can create such a disordered shell on the crystalline anatase core. Oriented $TiO_2$ NTs are chosen due to their high aspect ratio and unidirectional alignment, making them the ideal structure for diverse applications.[2,15,16] A distinct advantage of this method to fabricate ordered black $TiO_2$ NTs over others, such as high-pressure hydrogenation,[1] pulsed laser vaporization,[12] and electrochemical reduction,[17] is its simplicity and excellent control of crystallinity without breaking the nanoarrays. The black $TiO_2$ NTs thus obtained significantly enhance the optical response with a continuous spectrum of photoabsorption from UV to near-infrared. To fully understand the origin of this outstanding photoresponse, we have conducted careful surface and bulk characterization of these black $TiO_2$ NTs. X-ray absorption near-edge structure (XANES) and resonant inelastic scattering (RIXS) in combination with X-ray photoelectron spectroscopy (XPS) are employed to reveal the electronic and structural properties of and the differences between the amorphous shell and the crystalline core of the black $TiO_2$ NTs. XANES is elemental specific, which probes conduction band (unoccupied density of states) and the local chemical environment (e.g., local symmetry, oxidation state, etc.) via core-excitation by tracking the absorption coefficient while tuning the photon energy across the absorption edge of interest (excitation to bound, quasi-bound, and continuum states with well-defined angular momentum and chemical characteristics); thus, samples with either long (crystalline) or short-range (amorphous) order can be analyzed. RIXS, on the other hand, provides mapping of the valence band (occupied density of states) contribution of the excited atom in the ground state (it is valid under the single particle approximation, and this is often the case in low Z systems) via the almost concerted X-ray absorption and emission processes. Because the excitation is in the vicinity of the threshold, the core−hole effect involved in RIXS is negligible.[18] Herein, surface-sensitive XANES (using total electron yield) coupled with XPS are used to provide chemical information on the amorphous shell, whereas bulk-sensitive XANES (using X-ray partial fluorescence yield) in combination with RIXS are utilized to elucidate the photoabsorption properties, hence, structure and bonding of the anatase core.

## EXPERIMENTAL SECTION

**Sample Preparation.** Vertically aligned $TiO_2$ NTs with preferred geometry and alignment were prepared using a two-step electrochemical anodization process. A custom-made two-electrode cell was constructed using a Ti foil (0.1 mm in thickness, Goodfellow) with a surface area of 1 cm × 2 cm as the anode and a Pt wire as the cathode. The Ti foil was first rinsed by deionized water followed by absolute ethanol; then, Ti anodization was conducted at 50 V (Hewlett-Packard 6209B DC power supply) for 4 h to initiate the first NT layer growth with an electrolyte consisting of 0.3 wt % $NH_4F$ (98%, Alfa Aesar), 2 vol % $H_2O$, and ethylene glycol. Once finished, the Ti sheet was soaked in 1 M HCl for 5 min to peel off the first NT layer and then rinsed with deionized water and absolute ethanol. Subsequently, the refreshed sheet was used for the second Ti anodization at 50 V for 30 min using the same but fresh batch of the electrolyte as in the first step. Finally, the product NT was rinsed with absolute ethanol several times to remove the excessive electrolyte and then dried with $N_2$ gas. The as-prepared (or as-grown) NT is denoted APNT. Then, it was cut into 4 pieces. Two were kept as APNT, and two were annealed in ambient air at 450 °C for 2 h with a ramping rate of 5 °C/min to induce the crystallization of NTs, which are denoted NT450; after that, the annealing of NT450 (one piece) and APNT (one piece) in $NH_3$ was carried out simultaneously at 450 °C for 2 h to obtain N-doped NT450 and N-doped as-prepared NT, henceforth denoted NNT450 and NNT, respectively. $NH_3$ annealing was performed using a tube furnace. The tube was first purged with pure Ar with a gas flow of 10 mL/min for 10 min, and then the samples (one NT450 and one APNT) were heated under an $NH_3$ gas flow of 100 mL/min to atmospheric pressure with a ramping rate of 5 °C/min. Excessive $NH_3$ gas was bubbled through water.

**Characterization.** Scanning electron microscopy (SEM) images were recorded using a LEO (Zeiss) 1540 XB SEM. The microscopic NT structure was examined by high-resolution transmission electron microscopy (HRTEM, FEI Quanta FRG 200F) operating at 200 kV. X-ray diffraction (XRD, PANalytical Empyrean) was used to characterize the crystal structures of various NT samples. Room temperature UV−vis diffuse reflectance spectroscopy was recorded in the wavelength range of 300−800 nm using a Lambda 750 spectrophotometer (Perking Elmer). X-ray photoemission spectroscopy (XPS, Kratos Axis Ultra DLD, monochromatic Al K$\alpha$) was performed in an ultrahigh vacuum to characterize the electronic structures of various samples; the binding energy was calibrated to the C 1s reference peak at 284.5 eV. The resulting XPS data was fitted using software XPS PEAK 4.1.

Synchrotron experiments were performed at both the Canadian Light Source (CLS, Saskatoon, SK, Canada) and the Advanced Light Source (ALS), Lawrence Berkeley National Laboratory (LBNL, Berkeley, CA, US). Ti $L_{3,2}$-edge, O K-edge, and N K-edge XANES were measured using the Spherical Grating Monochromator (SGM) beamline at CLS with an energy resolution $E/\Delta E > 5000$.[19] Total electron yield (TEY) and partial fluorescence yield (PFY, collected from the element-specific fluorescence channel using an SSD detector) were used for data collection. All XANES spectra were normalized to the incident photon flux. Ti 2p RIXS spectra and some of the Ti $L_{3,2}$-edge and O K-edge XANES were collected at beamlines 6.3.2.1 and 8.0.1 of the ALS, where a high resolution grazing-incidence grating spectrometer with a 0.4 eV resolution was used.[20]

## RESULTS AND DISCUSSION

The high-resolution TEM (HRTEM) images in Figure 1 together with the SEM results (Figure S1) clearly show the well-shaped nanotubular morphology with a tube wall thickness of ∼30 nm. By air annealing of the as-prepared NTs (APNT) at


DOI: 10.1021/acs.chemmater.6b01673
Chem. Mater. 2016, 28, 4467−4475

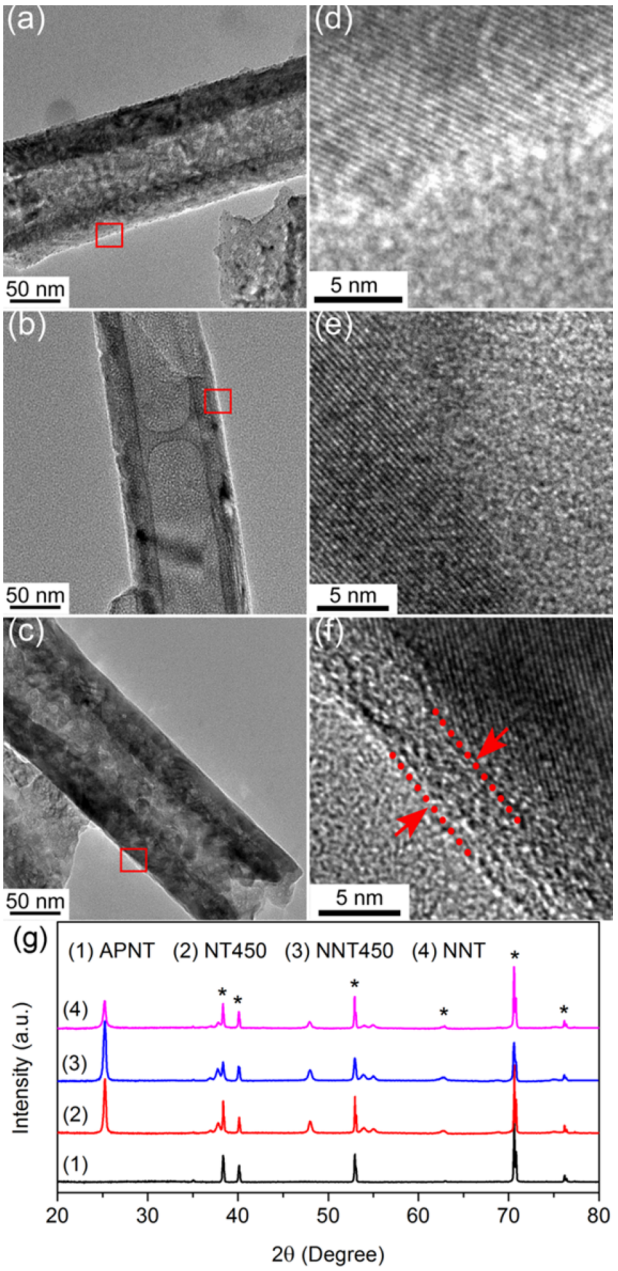


**Figure 1.** TEM/HRTEM images of NT450 (a/d), NNT450 (b/e), and NNT (c/f) where the location of shown HRTEM images are indicated in their corresonding TEM images with red rectangles. (g) XRD patterns of (1) APNT, (2) NT450, (3) NNT450, and (4) NNT. Diffraction peaks labeled with an asterisk (*) are attributed to the Ti substrate (JCPDS 44-1294).

450 °C, we obtain NT450 (Figure 1a and d), which displays the crystallized NTs. Further annealing of NT450 at 450 °C in $NH_3$ yields NNT450 (Figure 1b and e), which maintains its crystallinity compared to that of NT450. In contrast, $NH_3$ annealing of the as-grown NTs at 450 °C directly without air annealing, NNT, yields an amorphous outer layer with a thickness of ∼4 nm (on both the inner and outer wall of the tube) encapsulating a crystalline core, as shown in Figure 1f. The corresponding diffraction patterns of APNT, NT450, NNT450, and NNT are illustrated in Figure 1g. APNT only shows diffraction peaks from the Ti foil (JCPDS 44-1294), indicating the amorphous nature of these as-grown NTs. Once annealed, NT450, NNT450, and NNT all exhibit the anatase $TiO_2$ (JCPDS 65-5714) characteristic peaks as well as the strong signal from Ti substrate; no trace of a secondary phase (e.g., titanium oxynitride or titanium nitride) is observed in both NNT450 and NNT. However, the anatase peak intensity in NNT is much weaker than that of NT450 and NNT450, which suggests the decrease of crystallinity is due to the surface amorphization of NTs, consistent with the HRTEM result in Figure 1f.

Herein, the first important innovation of this work is the synthesis of anatase-core−amorphous-shell $TiO_2$ NTs by $NH_3$ annealing from amorphous phase. Figure 2 illustrates the main

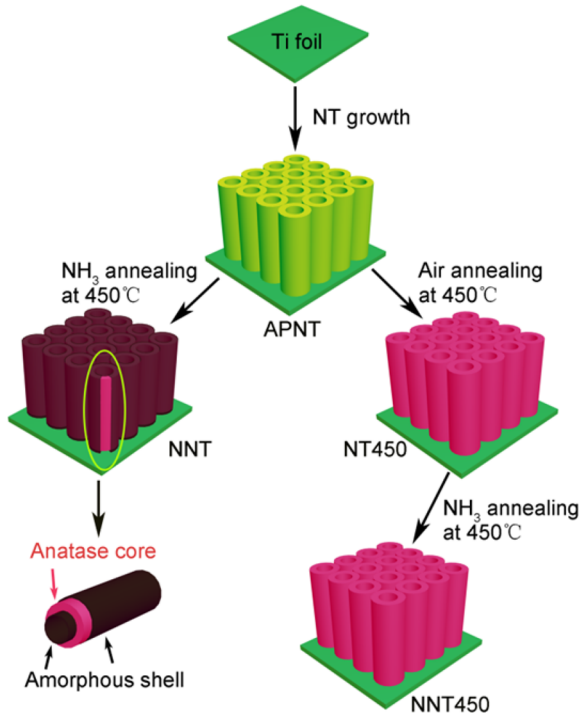


**Figure 2.** Schematic diagram of $TiO_2$ NT growth together with subsequent air and $NH_3$ annealing to fabricate NT450, NNT450, and NNT.

steps for the growth of $TiO_2$ NTs and postannealing for crystallization. The first step is the growth of vertically aligned amorphous NTs (Figure S1) by electrochemical anodization on a refreshed Ti foil. Clearly, after air annealing at 450 °C followed by $NH_3$ annealing at 450 °C, both NT450 and NNT450 are fully crystallized to the anatase $TiO_2$ phase. In comparison, $NH_3$ annealing of amorphous NTs (APNT) at 450 °C produces the new core−shell heterostructure of NNT with an amorphous surface (inner and outer shells) and a crystalline anatase core.

UV−vis diffuse reflectance spectroscopy was performed to examine the photoabsorption capability of core−shell NTs. As shown in Figure 3, bare anatase $TiO_2$ NTs (NT450) mainly absorb UV light where the absorption edge is located at ∼380 nm associated with the typical band gap of pure anatase $TiO_2$ (∼3.2 eV). After $NH_3$ annealing of NT450, NNT450 exhibits a slight enhancement of UV absorption and a sharp increase of absorption in the visible region, showing a broad band centered at ∼600 nm. By contrast, NNT with a core−shell heterostructure significantly harvests the entire visible wavelength. It starts to absorb continuously from the UV region and


DOI: 10.1021/acs.chemmater.6b01673
Chem. Mater. 2016, 28, 4467−4475

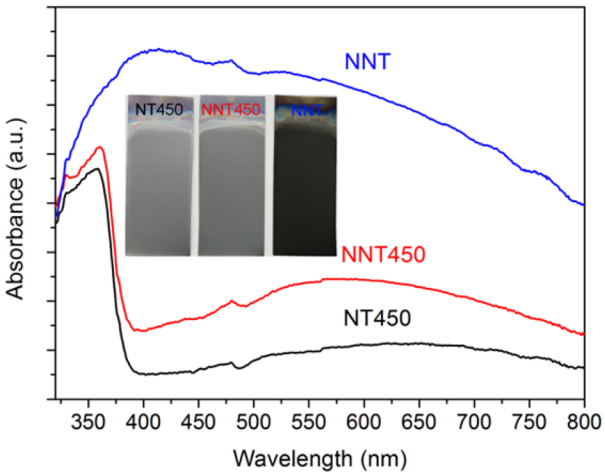


**Figure 3.** UV−vis diffuse reflectance spectra of NT450, NNT450, and NNT. The inset shows their different colors.

extends to the visible and then near-infrared region, suggesting the presence of a significant state in the band gap and band gap reduction of NNT compared to those of NT450 and NNT450.[1,8,14,21] Such light absorption enhancement is consistent with the dark black color of NNT as shown in the inset of Figure 3. In addtion, it is worth noting that the black color of NNT remains unchanged over 10 months after its synthesis in line with its photoabsorption behavior (Figure S2), suggesting the robust air-stability of the as-made black $TiO_2$ NTs.

The intense light absorption accomplished by NNT evidently suggests the establishment of a synergistic interaction between its amorphous shell and anatase crystalline core. Characterizations on the surface and in the bulk should be conducted carefully and preferentially to elucidate the origin of the excellent visible light capture. In this work, we utilize X-ray absorption near-edge structure (XANES) with detection modes of total electron yield (TEY) and partial fluorescence yield (PFY). TEY is surface-sensitive because it collects mainly secondary electrons from the NT surface with an electron escape depth of ∼4 nm (a dimension that matches the thickness of the amorphous phase in Figure 1g), whereas PFY is bulk-sensitive collecting element-specific fluorescent X-rays with an attenuation length at least 2 orders of magnitude larger than secondary electrons.[22] Therefore, TEY and PFY XANES in the soft X-ray region as in this case can be applied to comparatively analyze the electronic structure corresponding to the amorphous shell and the anatase core of NNT, respectively.

TEY and PFY XANES spectra of relevant samples at the Ti $L_{3,2}$-edge are shown in Figure 4, in which samples of $Ti_2O_3$ ($3d^1$, Sigma-Aldrich), anatase, and rutile $TiO_2$ ($3d^0$, Sigma-Aldrich) are used as standards for comparison. It should be mentioned that the PFY XANES in Figure 4b gets damped compared to TEY in Figure 4a due to self-absorption.[22] Generally, Ti $L_{3,2}$-edge probes electron transitions from Ti 2p core states to unoccupied states of Ti 3d character. It includes the two pre-edge features (peaks m and n), where their origin can be assigned to core-hole−d-electron interactions,[23,24] and the Ti $L_3$-edge (peaks a−c) and $L_2$-edge (peaks d and e) are due to electronic transitions from the spin−orbit split Ti $2p_{3/2}$ and $2p_{1/2}$ initial states, respectively, to the Ti 3d final states. Peak splitting into two well-resolved $t_{2g}$ and $e_g$ peaks within both the Ti $L_3$-edge and $L_2$-edge results from crystal field

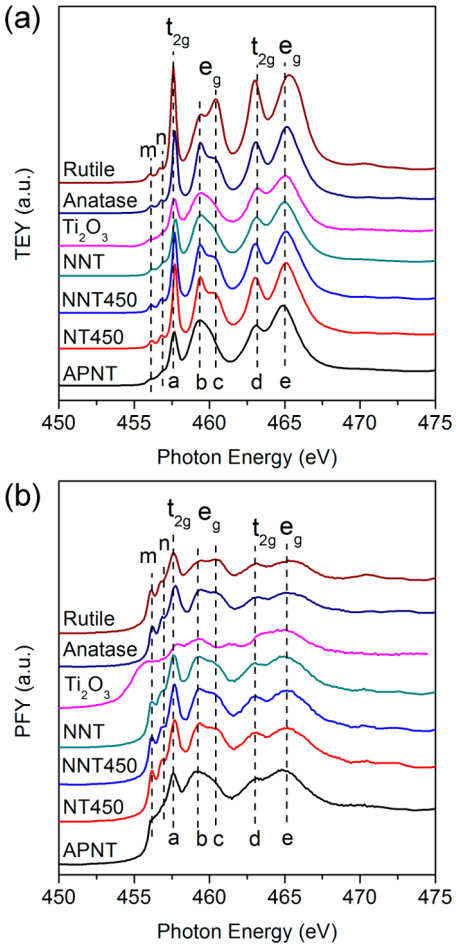


**Figure 4.** Ti $L_{3,2}$-edge XANES spectra of APNT, NT450, NNT450, and NNT in comparison with that of $Ti_2O_3$, anatase, and rutile standards as recorded in TEY (a) and PFY (b) modes.

splitting. Most importantly, the further splitting of $e_g$ peak (into peaks b and c) at the Ti $L_3$-edge is attributed to the local tetragonal distortion at the Ti site of the $TiO_6$ octahedron[25] or, alternatively, the long-range (nonlocal) distortion of $TiO_6$ octahedron connectivity.[26] Moreover, the extent of the $e_g$ peak splitting is also related to the oxidation state of Ti, i.e., that experimentally, the lesser resolved peaks b and c indicate a lower Ti oxidation, which implies the presence of some Ti 3d character.[27] Indeed, Figure 4a shows that different local distortions of $TiO_6$ from $O_h$ symmetry yields different Ti $L_3$-edge $e_g$ peak splitting behaviors between anatase ($D_{2d}$) and rutile ($D_{2h}$) $TiO_2$. Whereas the former shows a more intense feature b over c, the latter exhibits the reverse trend. Furthermore, with the decrease of Ti oxidation from $TiO_2$ ($3d^0$ for both anatase and rutile) to $Ti_2O_3$ ($3d^1$), the nominal gains of 0 and 1 electron occur, respectively, in the Ti 3d-$t_{2g}$ orbital (or d band). These electron filling processes result in the decrease of Ti 3d-$t_{2g}$ unoccupied states and further reduction in symmetry due to Jahn−Teller distortion, which together with exchange interaction would result in peak width broadening.[28] Concomitantly, the relevant $t_{2g}$ (peaks a and d) intensity decreases; then, the reduction of $t_{2g}/e_g$ intensity ratio as well as the less resolved $e_g$ peak splitting at the Ti $L_3$-edge of $Ti_2O_3$ are clearly shown in Figure 4a.[27] Nevertheless, it is worth mentioning that although the $Ti_2O_3$ standard in this work is purchased freshly from Sigma-Aldrich and used for the first


DOI: 10.1021/acs.chemmater.6b01673
Chem. Mater. 2016, 28, 4467−4475

time, it appears to be oxidized on its surface by clearly presenting the distinct TEY XANES (Figure 4a and Figure S3a) with its PFY spectrum (Figure 4b and Figure S3b) from the bulk, which shows a more consistent XANES profile with previous studies,[12,29] suggesting the severe instability of the $Ti_2O_3$ standard in ambient air.

Compared to the standards, both NT450 and NNT450 in Figure 4 display the anatase fine structure both on the surface and in the bulk, which in line with XRD analysis (Figure 1g) demonstrates their crystalline anatase structure. As for the core−shell NNT, although its core presents an anatase PFY XANES as expected, its amorphous shell, together with APNT, exhibits a TEY XANES pattern, which resembles that of the oxidized $Ti_2O_3$ standard, showing the absence of Ti $L_3$-$e_g$ peak splitting and a decrease of the $t_{2g}/e_g$ intensity ratio. This confirms that the Ti oxidation state on the NNT surface is partially reduced from $Ti^{4+}$. Also, note that the reduction of $Ti^{4+}$ in APNT is due to the self-doped $F^-$ ions from Ti anodization as reported in our previous work.[30] Results of TEY and PFY XANES recorded at the O K-edge (Figure S3) echo the above analysis at the Ti $L_{3,2}$-edge.

The areas under the curve in the resonance just above the threshold of the Ti $L_{3,2}$-edge and O K-edge XANES represent the densities of the unoccupied states of orbitals being probed. For example, Ti 3d unoccupied states or d holes are proportional to the area under 2p-to-3d resonance at the Ti $L_{3,2}$-edge. Because the first two strong resonances at the O K-edge (pre-edge, Figure S3) originate from electron transitions from O 1s states to O 2p-Ti 3d hybridized unoccupied states,[22] areas under relevant resonances at both the Ti $L_{3,2}$-edge and the O K-edge are proportional to the unoccupied states of the Ti 3d character (d holes). Thus, the larger the area, the higher the density of the Ti 3d unoccupied states and, hence, the higher the Ti oxidation state.

A detailed analysis has been performed by comparing the Ti $L_{3,2}$-edge and O K-edge XANES (normalized to unity at the same energy above the edge) of NNT to those of NNT450 and NT450. The results are shown in Figure S4; the areas under the Ti $L_{3,2}$-edge and O K-edge resonances integrated over the same region exhibit a trend of increasing intensity from NNT to NNT450 to NT450. Areas integrated from NNT450 are slightly lower than those of NT450, whereas the areas of NNT, especially those revealed from TEY XANES (Figure S4a and c), are sharply reduced compared to those of the other two. Therefore, it is clear that the Ti oxidation state in both the amorphous shell and anatase core of NNT has been reduced from $Ti^{4+}$, especially in the amorphous shell. Additionally, the difference revealed by the TEY and PFY XANES of NNT at the Ti $L_{3,2}$-edge (Figure 4) and O K-edge (Figure S3) clearly demonstrates the dissimilar electronic structure of its amorphous shell and crystalline core. Whereas the latter shows a long-range order and typical characteristics of anatase $TiO_2$ with a slight reduction of $Ti^{4+}$, the former exhibits a more dramatic effect with the presence of a larger amount of $Ti^{3+}$. Accordingly, the production of $Ti^{3+}$ has been assigned to a color center and mainly responsible for visible light absorption,[8,31−33] consistent with the dark black color of NNT and its continuous UV-to-near-infared absorption spectrum (Figure 3).

To further confirm the average chemical compostion of the reduced amorphous surface of NNT, we performed X-ray photoelectron spectroscopy (XPS). Note that the typical detection depth of XPS is on the order of approximately nanometers,[34] which is only sensitive to the amorphous shell (Figure 1f). Three regions of interest (Ti, O, and N) were mainly examined, and their corresponding spectra are shown in Figure 5. A comparison among the normalized Ti 2p XPS

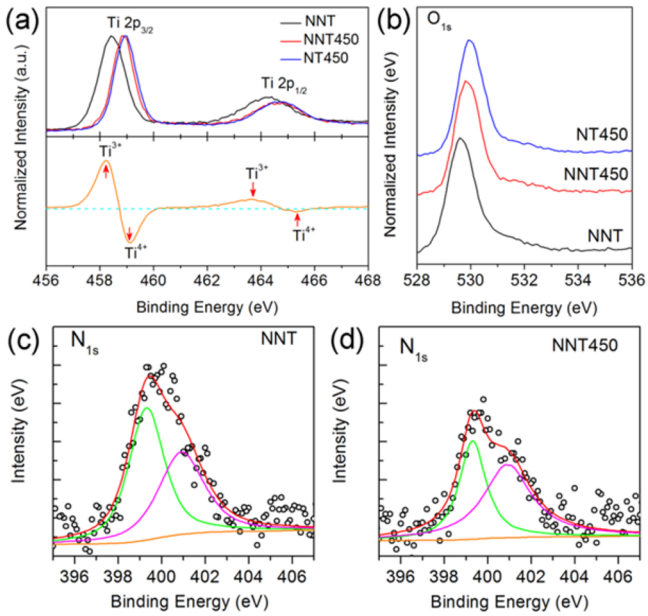


**Figure 5.** (a) Overlay of normalized (to maximum intensity) Ti 2p XPS spectra of NNT (black), NNT450 (red), and NT450 (blue) together with the difference spectrum by subtracting NNT with NT450. (b) Display of normalized O 1s XPS spectra of NNT, NNT450, and NT450 where the spectra of the latter two are vertically shifted for clarity. (c, d) N 1s XPS spectra of NNT and NNT450, respectively. Black circles are the experimental data, and red curves are the fitted XPS spectra in which the XPS spectra of NNT and NNT450 are deconvoluted into two peaks centered at 399.3 eV (green curve) and 400.9 eV (magenta curve). No N 1s signal is detected from NT450.

spectra of NNT, NNT450, and NT450 is illustrated in Figure 5a. A sharp peak centered at ∼458.9 eV and a broader peak at ∼464.7 eV are the characteristic Ti $2p_{3/2}$ and $2p_{1/2}$ peaks of $Ti^{4+}$, respectively,[1,35,36] and they are clearly presented in both NT450 and NNT450. In contrast, NNT shows a distinct shift to the lower binding energy region compared to the former two, indicating Ti of a lower oxidation state is present in the amorphous surface layer. To elucidate this difference, we subtracted the normalized Ti 2p spectrum of NNT (black) by that of NT450 (blue), and the difference curve is shown at the bottom of Figure 5a.[35] Clearly, two peaks are located at 458.2 and 463.7 eV in the difference spectrum, which are in accordance with the characteristic Ti $2p_{3/2}$ and $2p_{1/2}$ peaks of $Ti^{3+}$.[35,37] In evaluating the amount of $Ti^{3+}$ ions in the amorphous shell of NNT, deconvolution of its Ti 2p XPS (Figure S5) shows a $Ti^{3+}/Ti^{4+}$ atomic ratio of ∼1.2, illustrating that the amorphous shell has a composition close to the Magneli phase of $Ti_4O_7$.

Figure 5b displays the O 1s XPS spectra of NNT, NNT450, and NT450. All samples show asymmetry where the O 1s XPS spectrum of NT450 is deconvoluted to a sharp peak at ∼530 eV and a broad shoulder peak at ∼531.4 eV (Figure S6), which have been assigned to be the characteristic peaks of $TiO_2$ and Ti−OH, respectively.[1,35,36,38] Moreover, a closer observation of the O 1s XPS spectra indicates a negative shift in binding


DOI: 10.1021/acs.chemmater.6b01673
Chem. Mater. 2016, 28, 4467−4475

energy of O in NNT, which is probably due to the more negative charge states of O by N incorporation (via $NH_3$ annealing) as the change of bonding environment from O−Ti−O to O−Ti−N, and O is more electronegative than N. Similar findings have also been reported previously.[33]

The N 1s XPS spectra of NNT and NNT450 (Figure 5c and d) can be deconvoluted into two peaks at 399.3 and 400.9 eV. The former can be assigned to anionic N-doping in $TiO_2$ as O−Ti−N linkages (substitutional), whereas the latter is attributed to oxidized N in the form of Ti−O−N or Ti−N−O linkages (interstitial).[39,40] No sign of TiN is observed as its typical binding energy value is at ∼397 eV for N 1s states,[31,39] which is consistent with the XRD results in Figure 1g. The approximate atomic percentages of doped N in NNT and NNT450 are determined to be ∼5.1 and ∼4.7%, respectively, by calculating individual peak areas of Ti, O, and N and their respective atomic sensitivity factor. The area ratio of substitutional N peak to the interstitial N peak for NNT is ∼1.24, and this ratio decreases to ∼0.72 for NNT450, suggesting that substitutional doping is dominant in NNT whereas interstitial doping prevails in NNT450. More concrete evidence is provided at the N K-edge XANES in Figure S7, where the presence of a Ti−N bond is demonstrated both on the surface and in the bulk of NNT, whereas no Ti−N bond is observed on the surface of NNT450 and trapped $N_2$ is shown in the bulk.[41]

As for the crystalline core of NNT, although it displays a similar anatase structure with NNT450 and NT450, as revealed by PFY XANES (Figure 4b and Figure S3b), the decrease of the density of Ti unoccupied states in the bulk of NNT (Figure S4b and d) still shows its different electronic nature (e.g., oxygen-deficient $TiO_2$) from the other two. Hence, we further characterized the bulk of NNT, NNT450, and NT450 using bulk-sensitive resonant inelastic X-ray scattering (RIXS). As a photon-in−photon-out technique, RIXS usually can be used to characterize the bulk electronic structure (occupied densities of states) of materials at a few micrometers by the collection of characteristic X-ray emission from valence to shallow core transition ($L_\alpha$ and $K_\alpha$ from Ti $L_{3,2}$-edge and O K-edge, respectively) upon the creation of the core hole with excitation channels at or in the vicinity just above the edge.[18,20]

Figure 6 shows the four sets of RIXS spectra of NT450, NNT450, and NNT (bottom panel) with their corresponding excitation energies at the Ti $L_3$-edge XANES (top panel). All RIXS spectra are calibrated and displayed in an energy loss scale by subtracting their relevant excitation energy with the measured emission energy.[18,20,42,43] As noted in the literature,[20,42] once the excitation energy reaches the Ti 2p absorption threshold, two types of inelastic emission features are present in the Ti 2p RIXS spectrum in addition to the elastic peak with an energy loss at 0 eV. RIXS takes place in the regime of the crossover of the resonant Raman scattering (energy loss is a constant) and X-ray fluorescence (energy loss exhibits a disperson because fluorescence X-ray has a constant energy when excited above the threshold in the sudden regime).[18,20,30,42] As shown in Figure 6, the presence of a series of peaks below the elastic RIXS peak at 0 eV pictures the inelastic RIXS characters. The broad feature with an energy loss scale from 4 to 18 eV is attributed to contributions from both the Ti 3d → Ti 2p X-ray fluorescence (constant emission energy) and associated charge transfer excitations (constant energy loss) from O 2p to Ti 3d states. Note that those two components overlap with excitation energies at the Ti $L_3$-edge and will split into two once the excitation energy reaches the Ti

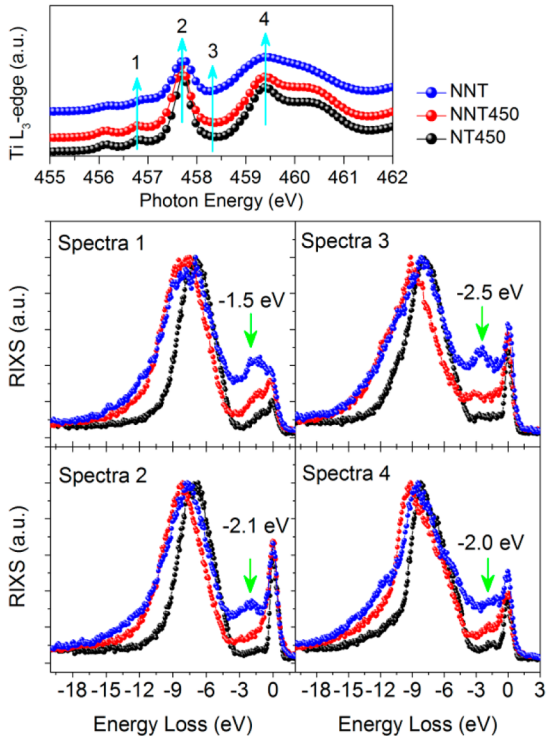


**Figure 6.** Ti 2p RIXS spectra (bottom) of NT450, NNT450, and NNT excited with selected photon energies corresponding to the Ti $L_3$-edge TEY XANES as shown on the top. The peak intensity of the four sets of RIXS spectra are normalized to their relevant Ti 3d → Ti 2p X-ray fluorescence.

$L_2$-edge (not shown here).[20,42] Most interestingly, a broad peak at ∼2 eV is also observed in both NNT and NNT450, but it is weak or nearly absent in NT450.

With the absence of these low energy inelastic scattering peaks in NT450, a noticeable increase of those features is observed in NNT450 at the energy loss scale between 0 and 4 eV. A further sharp increase in intensity of those peaks can be seen in NNT, especially for spectra 1 and 3, where their excitation energies locate at the pre-edge and the nonresonant absorption region of Ti $L_3$-edge between $t_{2g}$ (point 2) and $e_g$ (point 4) resonances, respectively. Apparently, the emergence of those extra low inelastic scattering features is facilitated by N incorporation. Because RIXS is analogous to resonant Raman scattering, which can detect energy transfers by electron transitions on the same atomic site,[6] these low inelastic energy peaks at ∼2 eV can thus be unambiguously traced to Ti d-d interband transtions from $Ti^{3+}$ ions reduced from $Ti^{4+}$ in $TiO_2$ upon N doping[20,42] i.e., that the Ti 3d orbital is partially occupied as a pseudo-$3d^1$ system. Further evidence, both experimental and theoretical, is provided by a Ti 2p RIXS study of $TiF_3$ ($3d^1$) showing an energy loss feature at ∼2 eV.[43] Additionally, as suggested by previous works,[12,20] the energy locations of points 1 and 3 are on the $t_{2g}$ and $e_g$ absorption resonances of $Ti^{3+}$, respectively, which explains the more intense d-d excitations observed in spectra 1 and 3 compared with those in spectra 2 and 4. The comparatively larger amount of N dopants in NNT than in NNT450 together with their dominant substitutional character disclosed in N 1s core level XPS (Figure 5c and d) and N K-edge XANES (Figure S7) account for the higher intensity of the $Ti^{3+}$ RIXS d-d transition feature in NNT. The slight energy loss variation (indicated by


DOI: 10.1021/acs.chemmater.6b01673
Chem. Mater. 2016, 28, 4467−4475

the green arrows) together with the broad character of these d-d excitation peaks suggest a distribution of as-obtained $Ti^{3+}$ states.[44] It is believed that $Ti^{3+}$ states in oxygen-deficient $TiO_2$ nanomaterials act as the photoabsorption centers, where electronic transitions from $Ti^{3+}$ intraband states to the conduction band of $TiO_2$ result from light absorption in the visible region.[9,32,33] Nevertheless, solid evidence regarding energy absorption by $Ti^{3+}$ had not been provided experimently until a recent study by Wang et al.[32] using two-photon photoemission spectroscopy (2PPE). Alternatively, this work using RIXS also demonstrates the energy absorption by $Ti^{3+}$, i.e., that d-d excitations show a dispersive energy transfer of ∼2 eV, which mainly contributes to the visible light capture of NNT450 with a broad absorption at ∼600 nm (Figure 3), and that the comparatively large amount of $Ti^{3+}$ bulk species of NNT coupled with the amorphous shell establishes the synergistic interaction with a continuous light absorption from UV to near-infrared.

Until now, conventional wisdom treated the disordered $TiO_2$ surface as the direct but nonspecific origin for the band gap narrowing and the corresponding visible light absorption of black $TiO_2$. In contrast to this notion, our results show that the amorphous shell has an average chemical composition of $Ti_4O_7$, which is a small band gap titanium oxide, and establishes the synergistic photoabsorption with the bulk, oxygen-deficient anatase $TiO_2$. We propose here that the composition of the amorphous surface of NNT resembles a highly disordered Magneli phase of $Ti_4O_7$ instead of the stoichiometric $TiO_2$ ($TiO_{2-x}$) as it is commonly referred to. Because surface $Ti^{3+}$ in stoichiometric $TiO_2$ is not stable in air as it is easily oxidized, only its bulk $Ti^{3+}$ is observed, accounting for the enhanced visible light absorption.[8,9,45] Consistent evidence of this is shown in NNT450, where only bulk $Ti^{3+}$ from N doping is detected by Ti 2p RIXS. These bulk $Ti^{3+}$ species exhibit an absorption energy associated with its visible light absorption. On the other hand, both TEY XANES (Figure 4a and Figure S3a) and Ti 2p XPS (Figure 5a) of NNT suggest that an equal amount of $Ti^{3+}$ and $Ti^{4+}$ is stabilizing the NT surface. The black color of NNT (Figure 3) unequivocally coincides with the high stability of $Ti^{3+}$ in the amorphous shell as it is known to be the color center of titanium oxide species.[8,32,33] Therefore, the formation of $Ti_4O_7$ can be justified. First of all, $Ti_4O_7$ with its mixed nature of $Ti^{3+}$ and $Ti^{4+}$ can preserve its $Ti^{3+}$ with high stability. In fact, Magneli phase $Ti_4O_7$ can be obtained via reduction of both anatase and rutile $TiO_2$,[46,47] which makes our proposal more convincing because this $Ti_4O_7$ layer is grown on the top of bulk anatase $TiO_2$. Second, whereas the attribution of band gap narrowing of black $TiO_2$ to the merging of band tail states with the valence band maximum and conduction band minimum is still controversial,[1,12] our proposed $Ti_4O_7$ is more resonable due to its much smaller band gap (∼1.5 eV) than that of anatase $TiO_2$ (∼3.2 eV).[48] Accordingly, the excellent visible light capture of NNT can mainly be attributed to the small band gap absorption of $Ti_4O_7$ in the amorphous surface synergetically coupled with photoabsorption by the distributed bulk $Ti^{3+}$ intraband states. Namely, it is likely that the amorphous surface layer stabilized by the anatase core provides a distribution of electronic states between these two band gap energies, leading to continuous absorption in the UV-to-near-infrared wavelength region. Admittedly, the involvement of slightly doped N (Figure 5c) as well as C (from residual electrolyte, Figure S8) on the surface of NNT can also contribute to its visible-infrared absorption secondarily.[3,9,31,49]

It is also important to mention that the crystallization of amorphous NTs in ambient $NH_3$ is the key for this functional dark black $TiO_2$ NT preparation. First, our previous work suggests that the as-grown amorphous NTs using $NH_4F$ as the electolye are self-doped with ∼14.5% (atomic percentage) of $F^-$ ions.[30] The release of those F species by breaking the Ti−F bonds can be achieved by thermal annealing. Thus, annealing of amorphous NTs in $NH_3$ (oxygen deficient) atomosphere can help the creation of massive oxygen vacancies via the breakage of Ti−F bonds. Second, compared to N doping in pure $TiO_2$, the introduction of N dopant in an oxygen-deficient $TiO_2$ lattice during the removal of F will become more convenient because these two processes occur simultaneously during $NH_3$ annealing. Concomitantly, N incorporation into the $TiO_2$ lattice via O substitution will significantly lower the formation energy of the oxygen vacancy to maintain the charge neutralization.[9] Therefore, oxygen vacancies in $TiO_2$ from all of these pathways will propagate and accumulate toward the NT surface during crystallization.[12] Consequently, $Ti_4O_7$ is attained on the NT surface once the stoichiometric $TiO_2$ is no longer sustained due to the excessive oxgyen vacancies. In addition, the amorphous nature of the NT surface mainly results from two processes. First, N doping together with oxygen vacancy formation causes the local distortion of $TiO_6$. Second, the accumulation of massive oxygen vacancies on the surface region could prevent its crystallization (long-range ordering);[21] thus, the NT surface keeps its original amorphous character with a short-range order, although the connectivity of $TiO_6$ will change, adopting a transitional configuration between $TiO_2$ and $Ti_4O_7$.

## ■ CONCLUSIONS

We have suceeded in using $NH_3$ annealing of the as-grown $TiO_2$ NTs prepared by Ti anodization to fabricate black $TiO_2$ NTs. Compared with the well-crystallized anatase $TiO_2$ NTs annealed in ambient air, then in $NH_3$, black $TiO_2$ NTs exhibit degradation in crystallinity on the surface, having a hetero-structure of an anatase core wrapped by an amorphous shell. This unique configuration of black $TiO_2$ NTs exhibits extraordinary light absorption behavior continuously covering the wavelength from UV to near-infrared. TEY (surface-sensitive) and PFY (bulk-sensitive) XANES analysis show that Ti in both the amorphous shell and the anatase core is heavily reduced. The former displays severe distortions of $TiO_6$ octahedra with a short-range order, whereas the latter maintains crystalline anatase. XPS confirms the TEY XANES result, which shows that the chemical composition is $Ti_4O_7$ in the amorphous shell. Ti 2p RIXS provides concrete evidence for the presence of bulk $Ti^{3+}$ by the observation of d-d excitations, which is absent in defect-free $TiO_2$. The energy loss at ∼2 eV with broadening corresponds to the broad visible light absorption at ∼600 nm. Consequently, the assembly of the $Ti^{3+}$-containing core of the anatase $TiO_{2-x}$ NT and its amorphous $Ti_4O_7$ surface establishes the significance of the synergistic effect responsible for the light absorption of black $TiO_2$ NTs. The key observation is the formation of amorphous $Ti_4O_7$ on the NT surface as a result of excessive accumulation of oxygen vacancies, which has high stability for preserving surface $Ti^{3+}$ and efficient light capture due to its variable band gap energy. This work provides new insights into the chemical nature of core−shell black $TiO_2$ NTs and thus will help develop more efficient nanostructures suitable for solar energy utilization. For example, optimization of the light capture of


DOI: 10.1021/acs.chemmater.6b01673
Chem. Mater. 2016, 28, 4467−4475

this core−shell system is underway in which variation of the N dopant concentration and thickness of the amorphous shell will be examined by controlling the reaction temperature, time, and $NH_3$ gas flow.

## ■ ASSOCIATED CONTENT

### Supporting Information

The Supporting Information is available free of charge on the ACS Publications website at DOI: 10.1021/acs.chemmater.6b01673.

SEM results (Figure S1), absorbance after air aging (Figure S2), O K-edge XANES analysis (Figure S3), overlay of Ti $L_{3,2}$-edge and O K-edge XANES (Figure S4), XPS fitting results of Ti 2p (Figure S5) and O 1s (Figure S6), N K-edge XANES analysis (Figure S7), and C 1s XPS spectra of as-grown and annealed samples (Figure S8) (PDF)

## ■ AUTHOR INFORMATION


### Corresponding Author

*E-mail: tsham@uwo.ca.


### Notes

The authors declare no competing financial interest.

## ■ ACKNOWLEDGMENTS

Research at the University of Western Ontario is supported by the Discovery Grant of the Natural Science and Engineering Research Council of Canada (NSERC), the Canada Research Chair (CRC) Program, the Canada Foundation for Innovation (CFI), and the Interdisciplinary Initiative (IDI) Grant of the University of Western Ontario (UWO). The work at the Canadian Light Source (CLS) is supported by CFI, NSERC, National Research council (NRC), Canadian Institute for Health Research (CIHR), and the University of Saskatchewan. The work at Advanced Light Source is supported by the Office of Basic Energy Sciences of the U.S. Department of Energy under Contract No. DE-AC02-05CH11231. We would like to thank Dr. T. Regier for technical support at the SGM beamline at CLS, and Mr. W. Xiao and Ms. B. Q. Wang for the assistance of sample preparation at UWO. J.L. acknowledges the receipt of support from the CLS Graduate Student Travel Support Program.

## ■ REFERENCES


(1) Chen, X. B.; Liu, L.; Yu, P. Y.; Mao, S. S. Increasing Solar Absorption for Photocatalysis with Black Hydrogenated Titanium Dioxide Nanocrystals. *Science* **2011**, *331*, 746−750.

(2) Ye, M. D.; Gong, J. J.; Lai, Y. K.; Lin, C. J.; Lin, Z. Q. High-Efficiency Photoelectrocatalytic Hydrogen Generation Enabled by Palladium Quantum Dots-Sensitized $TiO_2$ Nanotube Arrays. *J. Am. Chem. Soc.* **2012**, *134*, 15720−15723.

(3) Asahi, R.; Morikawa, T.; Ohwaki, T.; Aoki, K.; Taga, Y. Visible-Light Photocatalysis in Nitrogen-Doped Titanium Oxides. *Science* **2001**, *293*, 269−271.

(4) Wang, G. M.; Wang, H. Y.; Ling, Y. C.; Tang, Y. C.; Yang, X. Y.; Fitzmorris, R. C.; Wang, C. C.; Zhang, J. Z.; Li, Y. Hydrogen-Treated $TiO_2$ Nanowire Arrays for Photoelectrochemical Water Splitting. *Nano Lett.* **2011**, *11*, 3026−3033.

(5) Hu, Y. H. A Highly Efficient Photocatalyst−Hydrogenated Black $TiO_2$ for the Photocatalytic Splitting of Water. *Angew. Chem., Int. Ed.* **2012**, *51*, 12410−12412.

(6) Cheney, C. P.; Vilmercati, P.; Martin, E. W.; Chiodi, M.; Gavioli, L.; Regmi, M.; Eres, G.; Callcott, T. A.; Weitering, H. H.; Mannella, N. Origins of Electronic Band Gap Reduction in Cr/N Codoped $TiO_2$. *Phys. Rev. Lett.* **2014**, *112*, 036404.

(7) Gai, Y. Q.; Li, J. B.; Li, S. S.; Xia, J. B.; Wei, S. H. Design of Narrow-Gap $TiO_2$: A Passivated Codoping Approach for Enhanced Photoelectrochemical Activity. *Phys. Rev. Lett.* **2009**, *102*, 036402.

(8) Hoang, S.; Berglund, S. P.; Hahn, N. T.; Bard, A. J.; Mullins, C. B. Enhancing Visible Light Photo-Oxidation of Water with $TiO_2$ Nanowire Arrays *via* Cotreatment with $H_2$ and $NH_3$: Synergistic Effects between $Ti^{3+}$ and N. *J. Am. Chem. Soc.* **2012**, *134*, 3659−3662.

(9) Livraghi, S.; Paganini, M. C.; Giamello, E.; Selloni, A.; Di Valentin, C.; Pacchioni, G. Origin of Photoactivity of Nitrogen-Doped Titanium Dioxide under Visible Light. *J. Am. Chem. Soc.* **2006**, *128*, 15666−15671.

(10) Naldoni, A.; Allieta, M.; Santangelo, S.; Marelli, M.; Fabbri, F.; Cappelli, S.; Bianchi, C. L.; Psaro, R.; Dal Santo, V. Effect of Nature and Location of Defects on Bandgap Narrowing in Black $TiO_2$ Nanoparticles. *J. Am. Chem. Soc.* **2012**, *134*, 7600−7603.

(11) Liu, L.; Yu, P. Y.; Chen, X. B.; Mao, S. S.; Shen, D. Z. Hydrogenation and Disorder in Engineered Black $TiO_2$. *Phys. Rev. Lett.* **2013**, *111*, 065505.

(12) Tian, M. K.; Mahjouri-Samani, M.; Eres, G.; Sachan, R.; Yoon, M.; Chisholm, M. F.; Wang, K.; Puretzky, A. A.; Rouleau, C. M.; Geohegan, D. B.; Duscher, G. Structure and Formation Mechanism of Black $TiO_2$ Nanoparticles. *ACS Nano* **2015**, *9*, 10482−10488.

(13) Liu, N.; Schneider, C.; Freitag, D.; Venkatesan, U.; Marthala, V. R. R.; Hartmann, M.; Winter, B.; Spiecker, E.; Osvet, A.; Zolnhofer, E. M.; Meyer, K.; Nakajima, T.; Zhou, X. M.; Schmuki, P. Hydrogenated Anatase: Strong Photocatalytic Dihydrogen Evolution without the Use of A Co-Catalyst. *Angew. Chem., Int. Ed.* **2014**, *53*, 14201−14205.

(14) Chen, X.; Zhao, D. X.; Liu, K. W.; Wang, C. R.; Liu, L.; Li, B. H.; Zhang, Z. Z.; Shen, D. Z. Laser-Modified Black Titanium Oxide Nanospheres and Their Photocatalytic Activities under Visible Light. *ACS Appl. Mater. Interfaces* **2015**, *7*, 16070−16077.

(15) Fang, H. T.; Liu, M.; Wang, D. W.; Sun, T.; Guan, D. S.; Li, F.; Zhou, J. G.; Sham, T. K.; Cheng, H. M. Comparison of the Rate Capability of Nanostructured Amorphous and Anatase $TiO_2$ for Lithium Insertion using Anodic $TiO_2$ Nanotube Arrays. *Nanotechnology* **2009**, *20*, 225701.

(16) Mor, G. K.; Shankar, K.; Paulose, M.; Varghese, O. K.; Grimes, C. A. Use of Highly-Ordered $TiO_2$ Nanotube Arrays in Dye-Sensitized Solar Cells. *Nano Lett.* **2006**, *6*, 215−218.

(17) Yan, P. L.; Liu, G. J.; Ding, C. M.; Han, H. X.; Shi, J. Y.; Gan, Y.; Li, C. Photoelectrochemical Water Splitting Promoted with A Disordered Surface Layer Created by Electrochemical Reduction. *ACS Appl. Mater. Interfaces* **2015**, *7*, 3791−3796.

(18) van Schooneveld, M. M.; Suljoti, E.; Campos-Cuerva, C.; Gosselink, R. W.; van der Eerden, A. M. J.; Schlappa, J.; Zhou, K. J.; Monney, C.; Schmitt, T.; de Groot, F. M. F. Transition-Metal Nanoparticle Oxidation in A Chemically Nonhomogenous Environment Revealed by 2p3d Resonant X-ray Emission. *J. Phys. Chem. Lett.* **2013**, *4*, 1161−1166.

(19) Regier, T.; Paulsen, J.; Wright, G.; Coulthard, I.; Tan, K.; Sham, T. K.; Blyth, R. I. R. In Commissioning of the Spherical Grating Monochromator Soft X-Ray Spectroscopy Beamline at the Canadian Light Source. *AIP Conf. Proc.* **2006**, *879*, 473−476.

(20) Augustsson, A.; Henningsson, A.; Butorin, S. M.; Siegbahn, H.; Nordgren, J.; Guo, J. H. Lithium Ion Insertion in Nanoporous Anatase $TiO_2$ Studied with RIXS. *J. Chem. Phys.* **2003**, *119*, 3983−3987.

(21) Tan, H. Q.; Zhao, Z.; Niu, M.; Mao, C. Y.; Cao, D. P.; Cheng, D. J.; Feng, P. Y.; Sun, Z. C. A Facile and Versatile Method for Preparation of Colored $TiO_2$ with Enhanced Solar-Driven Photocatalytic Activity. *Nanoscale* **2014**, *6*, 10216−10223.

(22) Li, J.; Liu, L. J.; Sham, T. K. 2D XANES-XEOL Spectroscopy Studies of Morphology-Dependent Phase Transformation and Corresponding Luminescence from Hierarchical $TiO_2$ Nanostructures. *Chem. Mater.* **2015**, *27*, 3021−3029.

(23) Crocombette, J. P.; Jollet, F. Ti 2p X-Ray-Absorption in Titanium Dioxides ($TiO_2$) - the Influence of the Cation Site Environment. *J. Phys.: Condens. Matter* **1994**, *6*, 10811−10821.




DOI: 10.1021/acs.chemmater.6b01673
*Chem. Mater.* 2016, 28, 4467−4475

(24) Henderson, G. S.; Liu, X.; Fleet, M. E. A Ti L-Edge X-Ray Absorption Study of Ti-Silicate Glasses. *Phys. Chem. Miner.* **2002**, *29*, 32−42.
(25) Degroot, F. M. F.; Fuggle, J. C.; Thole, B. T.; Sawatzky, G. A. 2P X-Ray Absorption of 3D Transition-Metal Compounds - An Atomic Multiplet Description Including the Crystal-Field. *Phys. Rev. B: Condens. Matter Mater. Phys.* **1990**, *42*, 5459−5468.
(26) Kucheyev, S. O.; van Buuren, T.; Baumann, T. F.; Satcher, J. H.; Willey, T. M.; Meulenberg, R. W.; Felter, T. E.; Poco, J. F.; Gammon, S. A.; Terminello, L. J. Electronic Structure of Titania Aerogels from Soft X-Ray Absorption Spectroscopy. *Phys. Rev. B: Condens. Matter Mater. Phys.* **2004**, *69*, 245102.
(27) Kronawitter, C. X.; Bakke, J. R.; Wheeler, D. A.; Wang, W. C.; Chang, C.; Antoun, B. R.; Zhang, J. Z.; Guo, J.; Bent, S. F.; Mao, S. S.; Vayssieres, L. Electron Enrichment in 3d Transition Metal Oxide Hetero-Nanostructures. *Nano Lett.* **2011**, *11*, 3855−3861.
(28) Sham, T. K. Multiplet Splitting (Broadening) of the Ru $L_{2,3}$ Edge White Lines in the X-Ray Absorption Near Edge Spectra of $Ru(NH_3)_6Cl_3$. *J. Chem. Phys.* **1985**, *83*, 3222−3224.
(29) Stoyanov, E.; Langenhorst, F.; Steinle-Neumann, G. The Effect of Valence State and Site Geometry on Ti $L_3$, $L_2$ and O K Electron Energy-Loss Spectra of $Ti_xO_y$ Phases. *Am. Mineral.* **2007**, *92*, 577−586.
(30) Li, J.; Liu, C. H.; Ye, Y. F.; Zhu, J. F.; Wang, S. D.; Guo, J. H.; Sham, T. K. Tracking the Local Effect of Fluorine Self-Doping in Anodic $TiO_2$ Nanotubes. *J. Phys. Chem. C* **2016**, *120*, 4623−4628.
(31) Li, Z. D.; Wang, F.; Kvit, A.; Wang, X. D. Nitrogen Doped 3D Titanium Dioxide Nanorods Architecture with Significantly Enhanced Visible Light Photoactivity. *J. Phys. Chem. C* **2015**, *119*, 4397−4405.
(32) Wang, Z. Q.; Wen, B.; Hao, Q. Q.; Liu, L. M.; Zhou, C. Y.; Mao, X. C.; Lang, X. F.; Yin, W. J.; Dai, D. X.; Selloni, A.; Yang, X. M. Localized Excitation of $Ti^{3+}$ Ions in the Photoabsorption and Photocatalytic Activity of Reduced Rutile $TiO_2$. *J. Am. Chem. Soc.* **2015**, *137*, 9146−9152.
(33) Wang, J.; Tafen, D. N.; Lewis, J. P.; Hong, Z. L.; Manivannan, A.; Zhi, M. J.; Li, M.; Wu, N. Q. Origin of Photocatalytic Activity of Nitrogen-Doped $TiO_2$ Nanobelts. *J. Am. Chem. Soc.* **2009**, *131*, 12290−12297.
(34) Seah, M. P.; Dench, W. A. Quantitative Electron Spectroscopy of Surfaces: A Standard Data Base for Electron Inelastic Mean Free Paths in Solids. *Surf. Interface Anal.* **1979**, *1*, 2−11.
(35) Lu, X. H.; Wang, G. M.; Zhai, T.; Yu, M. H.; Gan, J. Y.; Tong, Y. X.; Li, Y. Hydrogenated $TiO_2$ Nanotube Arrays for Supercapacitors. *Nano Lett.* **2012**, *12*, 1690−1696.
(36) Sham, T. K.; Lazarus, M. S. X-Ray Photoelectron-Spectroscopy (XPS) Studies of Clean and Hydrated $TiO_2$ (Rutile) Surfaces. *Chem. Phys. Lett.* **1979**, *68*, 426−432.
(37) Werfel, F.; Brummer, O. Corundum Structure Oxides Studied by XPS. *Phys. Scr.* **1983**, *28*, 92−96.
(38) Lu, X. H.; Zheng, D. Z.; Zhai, T.; Liu, Z. Q.; Huang, Y. Y.; Xie, S. L.; Tong, Y. X. Facile Synthesis of Large-Area Manganese Oxide Nanorod Arrays as A High-Performance Electrochemical Supercapacitor. *Energy Environ. Sci.* **2011**, *4*, 2915−2921.
(39) Jagadale, T. C.; Takale, S. P.; Sonawane, R. S.; Joshi, H. M.; Patil, S. I.; Kale, B. B.; Ogale, S. B. N-Doped $TiO_2$ Nanoparticle Based Visible Light Photocatalyst by Modified Peroxide Sol-Gel Method. *J. Phys. Chem. C* **2008**, *112*, 14595−14602.
(40) Sathish, M.; Viswanathan, B.; Viswanath, R. P.; Gopinath, C. S. Synthesis, Characterization, Electronic Structure, and Photocatalytic Activity of Nitrogen-Doped $TiO_2$ Nanocatalyst. *Chem. Mater.* **2005**, *17*, 6349−6353.
(41) Hu, Y. F.; Sham, T. K.; Zou, Z.; Xu, G. Q.; Chan, L.; Yates, B. W.; Bancroft, G. M. A Study of Titanium Nitride Diffusion Barriers between Aluminium and Silicon by X-Ray Absorption Spectroscopy: the Si, Ti and N Results. *J. Synchrotron Radiat.* **2001**, *8*, 860−862.
(42) Higuchi, T.; Tsukamoto, T.; Watanabe, M.; Grush, M. M.; Callcott, T. A.; Perera, R. C.; Ederer, D. L.; Tokura, Y.; Harada, Y.; Tezuka, Y.; Shin, S. Crystal-Field Splitting and the On-Site Coulomb Energy of $La_xSr_{1-x}TiO_3$ from Resonant Soft-X-Ray Emission Spectroscopy. *Phys. Rev. B: Condens. Matter Mater. Phys.* **1999**, *60*, 7711−7714.
(43) Matsubara, M.; Uozumi, T.; Kotani, A.; Harada, Y.; Shin, S. Polarization Dependence of Resonant X-Ray Emission Spectra in Early Transition Metal Compounds. *J. Phys. Soc. Jpn.* **2000**, *69*, 1558−1565.
(44) Zhou, K. J.; Radovic, M.; Schlappa, J.; Strocov, V.; Frison, R.; Mesot, J.; Patthey, L.; Schmitt, T. Localized and Delocalized Ti 3d Carriers in $LaAlO_3/SrTiO_3$ Superlattices Revealed by Resonant Inelastic X-Ray Scattering. *Phys. Rev. B: Condens. Matter Mater. Phys.* **2011**, *83*, 201402.
(45) Wang, Y.; Feng, C. X.; Zhang, M.; Yang, J. J.; Zhang, Z. J. Visible Light Active N-Doped $TiO_2$ Prepared from Different Precursors: Origin of the Visible Light Absorption and Photoactivity. *Appl. Catal., B* **2011**, *104*, 268−274.
(46) Tang, C.; Zhou, D. B.; Zhang, Q. Synthesis and Characterization of Magneli Phases: Reduction of $TiO_2$ in A Decomposed $NH_3$ Atmosphere. *Mater. Lett.* **2012**, *79*, 42−44.
(47) Hauf, C.; Kniep, R.; Pfaff, G. Preparation of Various Titanium Suboxide Powders by Reduction of $TiO_2$ with Silicon. *J. Mater. Sci.* **1999**, *34*, 1287−1292.
(48) Zhong, X.; Rungger, I.; Zapol, P.; Heinonen, O. Electronic and Magnetic Properties of $Ti_4O_7$ Predicted by Self-Interaction-Corrected Density Functional Theory. *Phys. Rev. B: Condens. Matter Mater. Phys.* **2015**, *91*, 115143.
(49) Kurian, S.; Seo, H.; Jeon, H. Significant Enhancement in Visible Light Absorption of $TiO_2$ Nanotube Arrays by Surface Band Gap Tuning. *J. Phys. Chem. C* **2013**, *117*, 16811−16819.


DOI: 10.1021/acs.chemmater.6b01673
*Chem. Mater.* 2016, 28, 4467−4475